Orthogonal Smectic Layers Favour Nucleation through Diffusion-controlled Transformations: A Systematic Crystallization Kinetics Study

P. A. Kumar, Pisupati Swathi, and V. G. K. M. Pisipati

Centre for Liquid Crystal Research and Education (CLCRE), Faculty of Physical Sciences,
Nagarjuna University, Nagarjunanagar-522 510, India

Reprint requests to Prof. V. G. K. M. P.; E-mail: venkata_pisipati@hotmail.com

Systematic investigations of the crystallization kinetics of two representative compounds of *p*-phenylbenzylidene-*p*′-alkylanilines are performed, using differential scanning calorimetry, to study the influence of the kinetophase (occurs prior to the crystal phase) on the nucleation process. The dimensionality of the crystal growth and the related crystallization process are discussed in terms of the Avrami parameters *n* and *b*. The trend in the magnitude of the Avrami exponent *n* supports the occurrence of temperature-dependent transformations in the orthorhombic molecular array.

Key words: Crystallization Time; Kinetophase; Nucleation Process.

Introduction

Most polymorphic transformations and transformations involving simple decompositions into two phases are described by *nucleation and growth* [1, 2], in which nuclei of a phase are formed, followed by production of the new phase at a faster rate. In fact, phase transformations are extremely slow at the equilibrium temperatures and take place at measurable rates only after a certain degree of undercooling [3].

In orthogonal smectic phases the long axes of the molecules are perpendicular to the layer plane and the molecules rotate freely around these axes [4]. In tilted mesophases, however, the molecules experience hindered rotation around the layer normal. The variation in the layer thickness and the molecular rotations have a remarkable influence on the rate of crystallization. Similarly, among the orthogonal mesophases smectic-B and smectic-E, the significant difference of the molecular packing in the unit cell (hexagonal and orthorhombic) demonstrates the rotation of the molecules about the long molecular axes [5]. The unit cells in the smectic-B phase being just large enough to permit rotation, the molecules rotate relatively free when compared to the smectic-E phase [5]. The difference in the molecular rotation among these orthogonal phases is clearly caused to a great deal by the different crystallization kinetics performed in
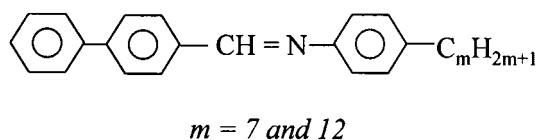

$$m = 7 \text{ and } 12$$

Fig. 1. Molecular structure of PB*n*A.

the smectogens exhibiting smectic-B and smectic-E phases as kinetophases. As a part of our systematic investigations on the kinetics of transformations in various liquid crystal systems, which include *p-n*-alkoxy benzylidene-*p*'-alkyl anilines (*n*O.*m*) [6], hydrogen-bonded systems [7, 8] and *p*-phenylbenzylidene-*p*'-alkylanilines (PB*n*A) [9], the present communication deals with the crystallization behaviour in the smectic-E kinetophase of the smectogens *p*-phenyl-benzylidene-*p*'-heptylaniline (PB7A) and *p*-phenyl-benzylidene-*p*'-dodecylaniline (PB12A), Fig. 1, and the mode of transformations in the orthogonal ordering is discussed in conjunction with the *n*O.*m* compounds exhibiting smectic-B as kinetophase.

Experimental

The synthetic procedures for the compounds PB7A and PB12A are described in [10]. A Perkin Elmer DSC-7 system is employed to measure the characteristic crystallization time and the corresponding enthalpies.
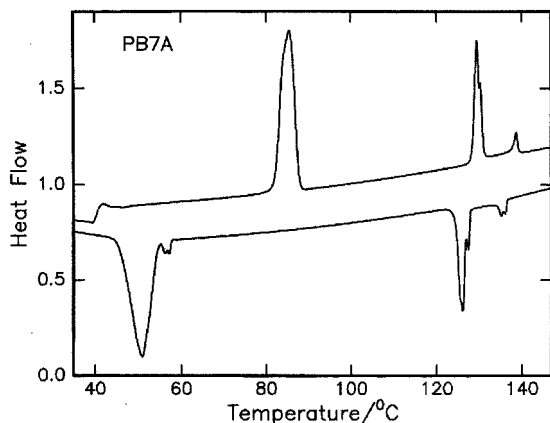
Fig. 2. The heating and cooling thermograms of PB7A.

Table 1. Transition temperatures (°C) of PB*n*A compounds in cooling cycle.

| Phase variants | Phase transition temperatures of TM and [DSC (ΔH/J/gm)] | | | | |
	I-N/A	N-A	A-B	B-E	E-Cryst.
PB7A:					
NABE	135.8	126.9	125.5	56.1	45.7
	[136.1(1.8)]	[127.5(19.3)]	[126.2*]	[57.2(1.7)]	[50.8(54.2)]
PB12A:					
ABE	125.6		116.4	81.7	67.3
	[124.3(13.3)]		[117.1(11.6)]	[*]	[76.7(121.1)]

* Transition peaks are not well resolved.

heated to the isotropic state at a scan rate of 10°C per minute. This process is repeated at each CT.

Results and Discussion

The phase variants of PB7A and PB12A are identified by their characteristic textures while cooling the isotropic melt using a polarizing thermal microscope [5]. The microscopic studies reveal the occurrence of marble texture (nematic), focal conic texture (smectic-A), and appearance of transient bars on the focal conic fans followed by smooth focal conic texture (smectic-B). These are common textures in both PB7A and PB12A. In addition to these phases, smectic-E phase with paramorphotic fan texture with concentric arcs across the fans is observed on cooling from smectic-B phase. The transition temperatures of the phases, observed through thermal microscopy, are found to agree reasonably with the corresponding DSC data (Table 1).

Rate of Crystallization

PB7A

The crystallization kinetics relating to the phase transitions from smectic-E to crystal have been performed at 60, 62, 64, 66, 68, and 70 °C. Figures 3 and 4 illustrate typical DSC endotherm profiles recorded for different time intervals at the CT's 60 and 70 °C. The heating curve recorded at $t = 0$ exhibits (Fig. 3) all the transitions except the melting transition. The appearance of a small peak is observed after holding the sample for 2 minutes, which is attributed to the crystal to Sm-E transition (melting transition). This peak attains its saturated value of enthalpy after 4.0 minutes suggesting a fast crystallization process. It is interesting to recall the trend in the growth of melting transition at the initial CT of the reported analogue, PB9A [9], where the formation of the crystal to
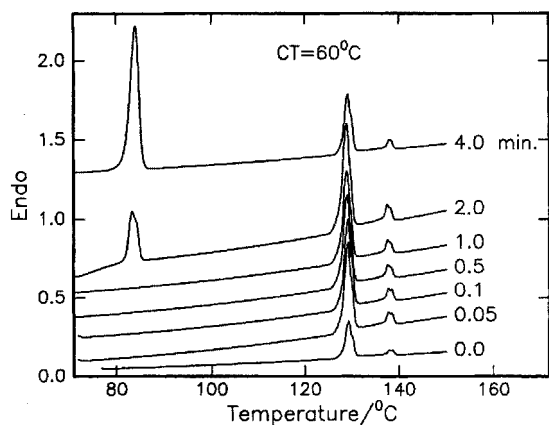
Selection of Crystallization Temperatures

As an example, the heating and cooling thermograms of PB7A are illustrated in Figure 2. On heating, the compound displays four distinct transitions: crystal to smectic-B (85.3 °C), smectic-B to smectic-A (129.2 °C), smectic-A to nematic (130.1 °C)*, and nematic to isotropic (138.5 °C) with the corresponding enthalpies 61.8, 19.6, (not well resolved)* and 12.4 J/g, respectively. On the other hand, the cooling exotherm shows the corresponding transitions at 136.1 °C (isotropic to nematic), 127.5 °C (nematic to smectic-A)*, 126.2 °C (smectic-A to smectic-B), 57.2 °C (smectic-B to smectic-E) and 50.8 °C (smectic-E to crystal) with heats of transitions 1.8, 19.3, (not well resolved)*, 1.7, and 54.2 J/g, respectively. The crystallization kinetics relating to the transition from smectic-E is performed over the crystallization range 60 to 70 °C. A glance at Fig. 2 reveals that once the phase transition from smectic-B to smectic-E is completed, the kinetics of the crystallization from smectic-E could be investigated over the temperature range between ($T_{\mathrm{cry-SmE}}$) and ($T_{\mathrm{SmE-cry}}$).

Typical DSC thermal scans for a given sample at each crystallization temperature (CT) of a liquid or solid crystal are described as follows. The sample is heated to its isotropic melt with a scan rate of 10 °C per minute. After holding for a considerable time for attaining thermal equilibrium, the sample is cooled to its predetermined CT at the same scan rate. After holding for a prerequisite time interval at a given CT, the endotherm peaks are recorded while the sample is

Fig. 3. DSC endotherm profiles of PB7A at 60 °C.

Fig. 4. DSC endotherm profiles of PB7A at 70 °C.

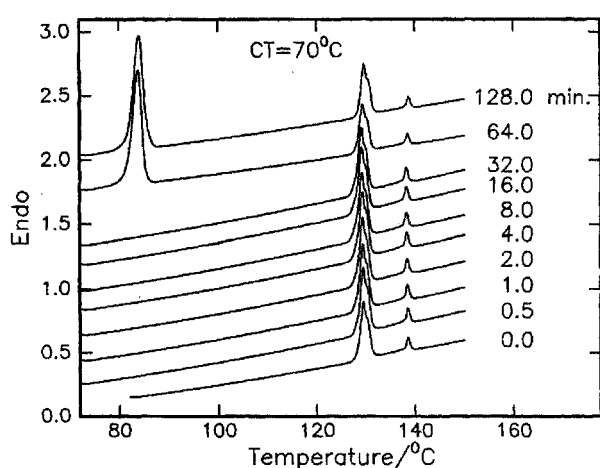Fig. 5. The heating and cooling thermograms of PB12A.

Fig. 6. DSC endotherm profiles of PB12A at 82 °C.

melting transition appears to begin after holding the sample for 0.8 minutes, and its growth continues until the time interval reaches 2.0 minutes. This clearly suggests the significant role of alkyl carbon number on the rate of crystallization. The endotherm profiles recorded at the CT's 62, 64, 66, 68, and 70°C showed a similar trend in the growth of the melting transition and attained saturation after 8.0, 16.0, 32.0, 64.0, and 128.0 minutes, respectively. A glance at Fig. 4 implies a delayed crystallization process at the final CT 70°C, owing to the characteristic crystallization time of 128.0 minutes.

PB12A

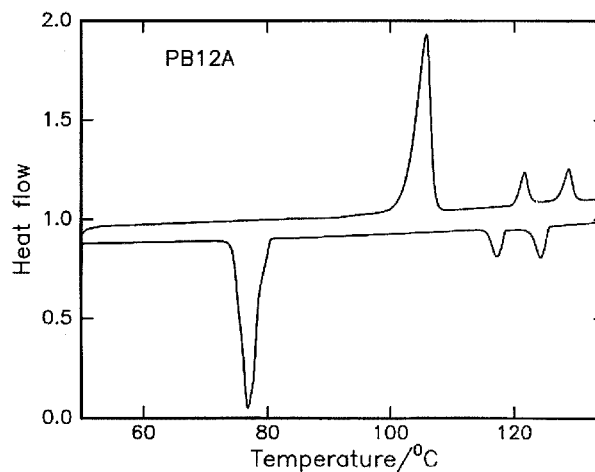Figure 5 represents heating and cooling thermograms of PB12A. The endotherm peaks are assigned to crystal to smectic-B (105.7 °C), smectic-B to smectic-A (121.6 °C), and smectic-A to isotropic (128.8 °C) transitions with their characteristic enthalpies 122.3, 11.9 and 13.3 J/g, respectively, while the exotherms reveal the phase transitions at 124.3 (isotropic to smectic-A) 117.1 (smectic-A to smectic-B) and 76.7 °C (smectic-E to crystal) with their heats of transitions 13.3, 11.6 and 121.1 J/g, respectively. However, the mono-tropic transition pertinent to smectic-B to smectic-E observed through thermal microscopy is not well resolved in the cooling cycle. From the observed melting and crystal transitions the kinetics studies relating to the transitions from smectic-E phase was carried out at the CT's 81, 82,
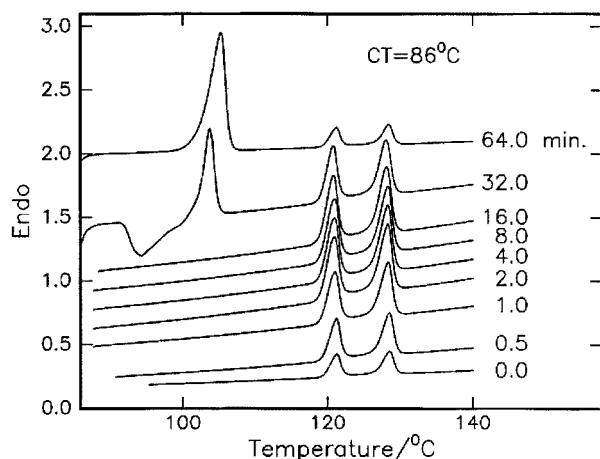
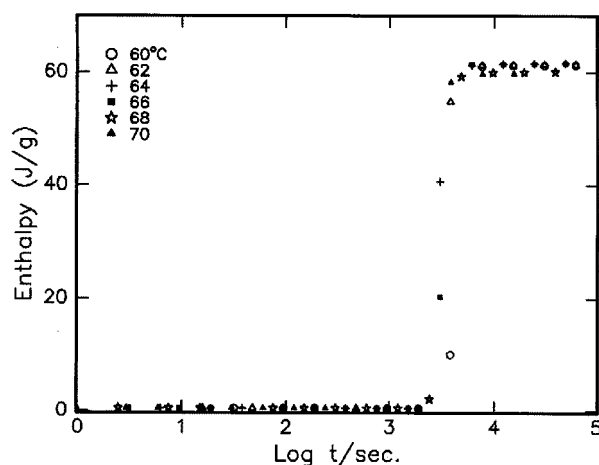Fig. 7. DSC endotherm profiles of PB12A at 86 °C.

Fig. 8. Heats of melting as a function of the logarithm of the annealing time of PB7A.
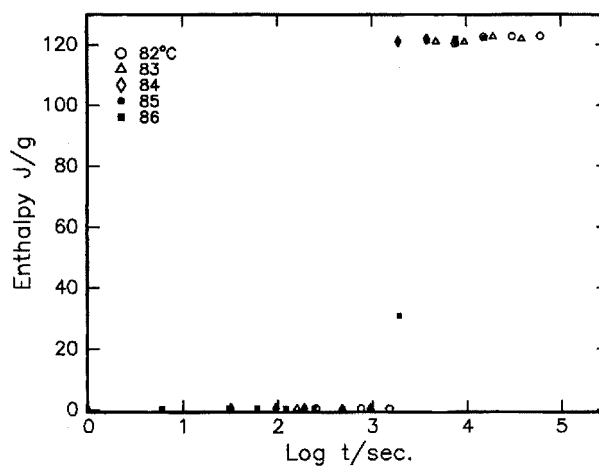
Fig. 9. Heats of melting as a function of the logarithm of the annealing time of PB12A.

83, 84, 85, and 86 °C. As expected, fast kinetics is observed at the lower CT's 81, 82, and 83 °C, and a relatively slow rate of crystallization was observed at the final temperatures. Typical endotherm profiles, recorded at 82 and 86 °C, are given in Figs. 6 and 7, respectively. A glance at these figures suggests a faster rate of crystallization at 82 °C, with the melting transition appearing suddenly with its saturated value of enthalpy after 1 minute. On the other hand, a sudden change in the rate of crystallization can be seen at the CT 86 °C, where a slow rate of crystallization is observed with the melting transition attaining its saturation after 64.0 minutes. Attempts have also been made to observe the growth of the melting transition at 87 °C, but the trend suggest that the kinetics is too slow, as the melting transition is not observed even after 256 minutes. This clearly suggests a delayed nucleation process operating on the higher temperature side of the crystal melting.

Crystallization Process

In order to study the crystallization process at each crystallization time, the enthalpy values for individual transitions of different time intervals are calculated for each CT, and the corresponding data are plotted against to the corresponding logarithm of time intervals for both compounds under study. Figures 8 and 9 show such plots for PB7A and PB12A, respectively. It is observed that these plots are identical in shape, apart from the shift on the log *t* axis, suggesting lim-itations of the rates of crystallization [2]. Further, it can be clearly seen that in the two compounds the growth of the melting peaks at the initial and final CT's follows a reverse trend. In other words, in PB7A a gradual formation of the melting peak is observed at lower temperature (60 °C), while in the case of PB12A the high CT (86 °C) favours a slow formation of the melting transition.

The Avrami equation [11]

$$x = 1 - \exp\{-(t/t^*)^n\}, \tag{1}$$

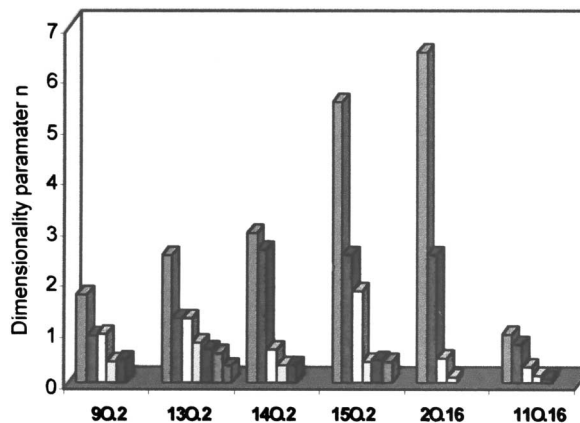where $t^* = b^{-1/n}$, is quite useful in differentiating the

Table 2. Measured Crystallization parameters for PB7A and PB12A.

Compound	CT (°C)	t^* (min)	x	n	b
PB7A	60	4.0	0.9861	1.069	$2.272 \cdot 10^{-1}$
	62	8.0	0.9895	0.57	$3.056 \cdot 10^{-1}$
	64	16.0	0.9939	0.319	$4.129 \cdot 10^{-1}$
	66	32.0	0.9934	0.157	$5.803 \cdot 10^{-1}$
	68	64.0	0.9688	0.054	$7.988 \cdot 10^{-1}$
	70	128.0	0.9655	0.026	$8.797 \cdot 10^{-1}$
PB12A	82	0.5	0.9834	8.197	$3.143 \cdot 10^{2}$
	83	0.5	0.9902	9.251	$6.092 \cdot 10^{2}$
	84	1.0	0.9897	4.576	$10.0 \cdot 10^{-1}$
	85	2.0	0.9908	2.345	$1.968 \cdot 10^{-1}$
	86	64.0	0.9909	0.0735	$7.366 \cdot 10^{-1}$

Fig. 10. The dimensionality parameter *n* as a function of the crystallization temperature of the *n*O.*m* compounds.

kind of nucleation mechanism operating at different CT's in various non-isothermal transformations. The characteristic time t^* can be determined experimentally at $t = t^*$, and x at a particular CT is deduced from the experimental data of $\Delta H / \Delta H_0$, where ΔH is the crystal melting heat measured at the time t and ΔH_0 is the maximum value obtained from the plateau of individual curves (Figs. 8 and 9). The values of n and b were calculated from (1) for each compound, and the data are included in Table 2.

At a particular CT the Avrami exponent n plays a crucial role in ascertaining the mode and class of transformations which occur when a stable low temperature phase grows out of a metastable mother phase in the form of small domains [3]. It is noticed that the dimensionality parameter n, varies from 1.069 to 0.026 in PB7A and from 8.296 to 0.073 in PB12A. As in the case of reported analogues [9], n follows a decreasing trend with increase of the CT's, suggesting the occurrence of different modes in the conversion process at each CT. A possible explanation for the occurrence of this crystallization behaviour may best be invoked on the basis of sporadic nucleation growth, which takes place as a homogeneous process over a constant period of time.

The value of b, which governs the nucleation mechanism, is calculated from the experimental data using (1). The magnitude of b is almost unaltered, 10^{-1}, at most of the CT's, which agrees well with the trend for the reported analogues [9]. Further, these values obtained for each compound, show a gradual increment with increasing CT (Table 2). This clearly indicates the existence of a unique crystallization mechanism operating over the entire thermal range of the crystallization.

Influence of the Crystallization Temperature and the End Chain Carbons on the Mode of Transformation

In order to understand the effective role of the CT on the transformation mode, a comparative study is made with the reported *n*O.*m* compounds [6] in terms of the varied magnitude of the Avrami exponent *n*.

It is interesting to note that the reported *n*O.*m* compounds exhibit two modes of transformation during the nucleation process, based on the observed magnitudes of *n* at the corresponding CT's [3]. Figure 10 represents the magnitudes of *n* as functions of the CT in *n*O.*m* compounds after the reappraisal of the values reported in [6]. For instance, 9O.2 reveals a diffusion-controlled transformation where the initial growth of particles nucleated only at the start of the transformation ($n = 1.71$ at 43 °C) while at the following CT's (CT = 45 and 47 °C; $n = 0.9$ and 0.95), the growth of these nucleated particles involves the formation of isolated plates or needles of finite size. Later, thickening of these plates with impinged edges [3] is observed at the final temperatures (CT = 49 and 51 °C; $n = 0.4$ and 0.43). In the case of 13O.2, at the initial temperature (CT = 55 °C; $n = 2.5$) the nucleation starts as the initial growth of particles with a constant rate followed by the growth of isolated plates or needles of finite size (CT = 56 and 57 °C; $n = 1.25$ and 1.25). At the final temperatures (CT = 58 - 62 °C) the crystal transformation involves the thickening of plates with impinged edges.

On the other hand, at the initial temperatures, the compounds 14O.2, 15O.2, and 2O.16 display diffusionless transformations [3] wherein the nucleation
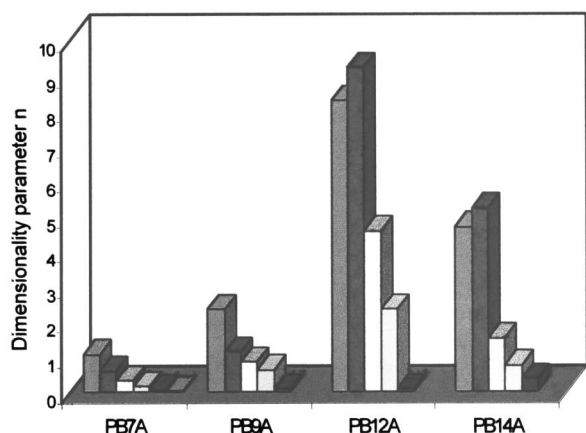
Fig. 11. The dimensionality parameter *n* as a function of the crystallization temperature of PB*n*A compounds.

starts with a constant rate at grain boundaries. At higher CT's the compounds show diffusion-controlled transformations involving the growth of isolated plates or needles of finite size. Further, it is worth to mention that the alkyl and / or alkoxy carbons show a remarkable impact on the mode of conversion. This can be realized by considering the magnitudes of *n* observed for 11O.16, where a diffusion-controlled transformation is seen as this compound reveals low magnitudes of *n* (< 1) at the initial temperatures. This, in fact, supports our previous experimental conclusion [6] towards the influence of the *n/m* ratio on the crystallization process in a more quantitative way. In other words, when *n/m* becomes almost unity (*n* = *m*) the crystal transformation follows a diffusion-controlled process leading to a delayed crystallization process.

In the case of present PB*n*A compounds, the magnitude of *n* across the CT's (Fig. 11) confirms the occurrence of two modes of transformation. This can be justified by the effective role of the flexible alkyl moiety on the nucleation process. In other words, it can be visualized from the active role of the phenyl moiety as a terminal functionality. As borne out by the data (Table 1), PB*n*A compounds with alkyl carbons equal to 7 and 9 (PB7A and PB9A) show diffusion-controlled transformations, which involve the initial growth of particles nucleated only at the start of the transformation and at the following CT's the growth of these nucleated particles leads to the formation of isolated plates or needles of finite size with impinged edges [3].

On the other hand, the higher homologues (PB12A and PB14A) reveal temperature-dependent transformations as in the case of higher members of the *n*O.*m* series (*n* > 11; *m* > 14). At the initial temperatures, these compounds follow a diffusionless transformation where the high magnitude of *m* prevails the nucleation, which starts with a constant rate at grain boundaries. At higher CT's, these compounds display diffusion-controlled transformations involving the formation and growth of isolated plates or needles of finite size.

Conclusion

The phase variant among the individual members of smectogens belonging to a similar class plays an effective role in the rate of crystallization. Our comprehensive crystallization kinetics investigations on various smectogens [6 - 9] enabled us to arrange both orthogonal and tilted kinetophases in increasing order of their crystallization time. It has been clearly emphasized that for kinetophases towards the crystal end favour fast rates of crystallization while a delayed kinetics is observed for those near to the isotropic melt. As expected, a faster rate of kinetics is observed for PB7A and PB12A when compared with the reported *n*O.*m* compounds [6] exhibiting the tilted kinetophase (12O.12 and 14O.14) where a slow rate of crystallization is observed.

The experimental results also confirm the influence of the degree of variation in the molecular rotation among the orthogonal phases (smectic-B in *n*O.*m* and smectic-E in PB*n*A) on the crystallization process in terms of varied magnitudes of the Avrami exponent *n*. It is also realized from the present study that an increase in alkyl carbon number of the aniline moiety delays the crystallization time. Nevertheless, the magnitude of the growth parameter *b* suggests a unique crystallization mechanism operating over a particular crystallization time. The low values of *n*, however, infer the occurrence of diffusion-controlled transformations in which the nucleation starts as an initial growth of particles in the form of plates or needles of finite size possessing impinged edges.

[1] F. P. Price and J. H. Wendorff, J. Phys. Chem. **75**, 2849 (1971); **76**, 276 (1972).

[2] Z. He, Y. Zhao, and A. Callie, Liq. Cryst. **23**, 317 (1997).

[3] C. N. R. Rao and K. J. Rao., Phase Transitions in Solids, Mc Graw Hill, U.S.A 1978.

[4] D. Demus, Liquid Crystals: Phase Types, Structures and Chemistry of Liquid Crystals, Springer, New York 1994.

[5] G. W. Gray and J. W. G. Goodby, Smectic Liquid Crystals-Textures and Structures, Leonard Hill, London 1984.

[6] P. A. Kumar, M. L. N. Madhu Mohan and V. G. K. M. Pisipati, Liq. Cryst. **27**, 727 (2000).

[7] P. Swathi, P. A. Kumar, and V. G. K. M. Pisipati Liq. Cryst. **28**, 1163 (2001); Liq. Cryst. 2001 (in press); Mol. Mater. 2001 (in press).

[8] M. Srinivasulu, P. V. V. Satyanarayana, P. A. Kumar, and V. G. K. M. Pisipati, Liq. Cryst. **28**, 1321 (2001); Z. Naturforsch. **56a**, 685 (2001); Mol. Mater 2001 (in press).

[9] Ch. Srinivas, P. N. Murty, P. Swathi, P. A. Kumar, and V. G. K. M. Pisipati Liq. Cryst. 2001 (in press).

[10] D. M. Potukuchi, S. Lakshminarayana, C. R. Prabhu and V. G. K. M. Pisipati Cryst. Res.Technol. **31**, 685 (1996).

[11] M. Avrami., J. Chem.Phys. **7**, 1103 (1939); J. Chem. Phys. **8**, 212 (1940).